Int. J. Advanced Design and Manufacturing Technology, 2025, Vol. 18, No. 2, pp. 1-8

DOI: 10.71644/admt.2025.873794 *ISSN: 2252-0406* *https://admt.isfahan.iau.ir*

Nonlinear Wheel Slip Control of Electric Vehicles with In-Wheel BLDC Motors

Majid Majidi[1, *]
Department of Mechanical Engineering, Qa.C., Islamic Azad University, Qazvin, Iran
E-mail: majid.majidi@iau.ac.ir
*Corresponding author

Pouyan Ahmadizadeh[2]
School of Automotive Engineering, Iran University of Science and Technology, Tehran, Iran
E-mail: p.ahmadizadeh@gmail.com

Received: 10 November 2024, Revised: 4 February 2025, Accepted: 10 March 2025

Abstract: This paper introduces a vehicle wheel slip tracking using an in-wheel BLDC (brushless direct current) motor. The control objective is to track a reference input wheel slip. The control architecture consists of a two-layer structure. In the upper level of the control system, the controller design is based on a sliding mode control strategy and generates the required torque for each wheel as the wheel slip tracks the reference value. In the lower level, the torque controller is a current controller with the duty cycle of the PWM (pulse width modulation) pulses to achieve the desired torque demanded by the upper level. In torque controller, a BLDC motor controller with a three-phase inverter is designed using Hall Effect sensor feedback and current sensors. The design is performed so that the wheel slip tracks any reference input wheel slip. Simulations are performed to demonstrate the effectiveness of the proposed two-layer controller.

Keywords: BLDC Motor, Sliding Mode Control, Wheel Slip Control

Biographical notes: Majid Majidi received his PhD in Automotive Engineering from Iran University of Science and Technology in 2015. He has worked as an assistant professor at the Department of Mechanical Engineering, Qazvin Islamic Azad University, since 2015. His current research interests include vehicle dynamics and control, modeling, simulation, and control of hybrid and electric vehicles. **Pouyan Ahmadizeh** received his PhD in Automotive Engineering from Iran University of Science and Technology in 2017. His current research interests include vehicle dynamics and control, hybrid and electric vehicles powertrain.

Research paper

1 INTRODUCTION

Electric motors have good performance for motion control applications since their torque response is quite fast and accurate. The application of in-wheel motors in hybrid or electric vehicles is an object of intense research activities, for some earlier studies [1-4]. In this way, the motor torque of each wheel can be controlled independently without requiring any additional actuators. Such an arrangement permits dynamic control to be realized using only software and delivers the benefits of the inherently rapid, precise torque controllability. For the lower layer controller, slip control is being done with the use of vehicle stability control known as DYC (direct yaw-moment control) in EVs (electric vehicles) [5-6]. In this approach, by using in-wheel motors, the anti-directional torque generation is applied on the left and right wheels [7-8]. The main difficulty arising in the design of a wheel slip control is due to the strong nonlinearity and uncertainty in the problem [9]. Therefore, sliding mode control is a preferable approach for this kind of problem because of its robustness. Sliding mode controllers have been designed previously for the purpose of controlling wheel slip [10]. For tracking a reference wheel slip by electrical motor, information on the longitudinal (tractive/braking) tire force of each wheel must be supplied to the controller. Since electrical motor torque is easily comprehensible, there exists little uncertainty in driving or braking torque generated by the motor, compared to that of an internal combustion engine or hydraulic brake. Therefore, a simple driving force observer can achieve a real-time observation of the driving/braking force between the tire and the road surface [11-12]. This paper describes the control method devised to enhance slip tracking for traction application of EVs. This paper proposes a wheel slip control method based on the feedback of wheel angular velocity, which is easily measured. If every wheel has a driving motor, this slip controller can be applied to every wheel. By maintaining the wheel slip at the desired level, the desired longitudinal (tractive) tire force is generated, and the desired longitudinal speed due to driving command is, therefore, achieved. The control algorithm developed in this paper uses a nonlinear tire model to provide the tire forces for simulation purposes.

2 MODELING

In this section, the dynamic models of the vehicle, wheel, and BLDC motors are presented to set up the control problem and simulation.

Vehicle Modeling

Vehicle models are available with several complexities. More complex models could have accurate results but take more simulation time. On the other hand, less complex models are simple for simulation but might have less accuracy. The models with basic properties of the system have often been preponderant for many applications and have reliable results. The vehicle model considered here for simulation purposes consists of 8 degrees of freedom (DOF). These include longitudinal and lateral motions, yaw and body roll motions, as well as the rotational dynamics of the four wheels. In addition, the steering system is assumed to be stiff, and the drive line dynamics is neglected for simplicity (driving/braking torques are thus applied directly to the wheels) [13]. Figure 1 shows the free-body form of the vehicle model, and "Fig. 2" shows the layout of the wheel dynamics.

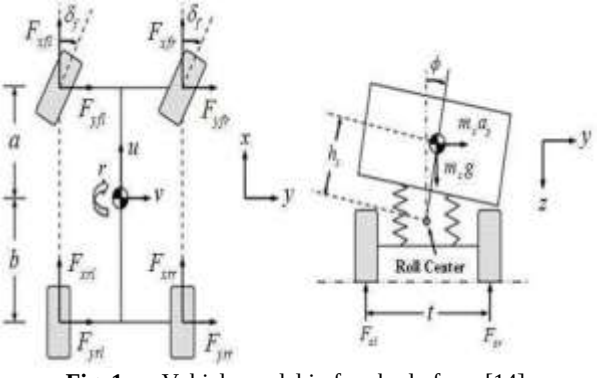

Fig. 1 Vehicle model in free-body form [14].

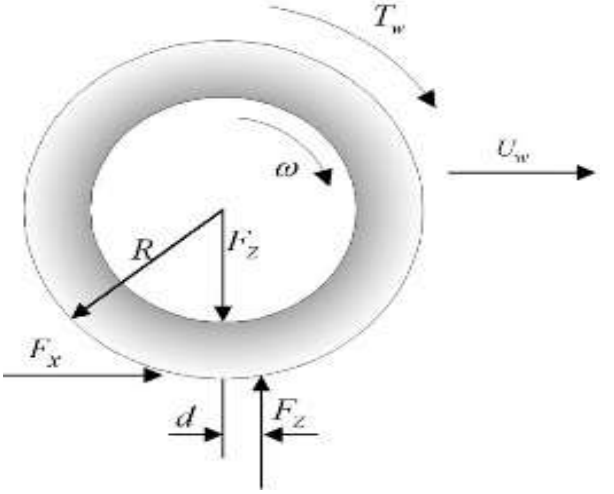

Fig 2. Wheel dynamics layout [14].

The Equation of wheel dynamics is needed for sliding mode control, that is:

$$\dot{\omega} = \frac{1}{J_w}\left(T_w - F_x R - F_z d\right) \tag{1}$$

Where J_w is the mass moment inertia of the wheel and connecting parts about the axis of rotation, T_w is the wheel torque, F_z and F_z are the wheel longitudinal and normal forces respectively, R is the wheel radius and d is the distance between the spin axis and the road vertical reaction force.

Tire Model

In order to simulate the tire model, the nonlinear magic formula tire [15] model with combined longitudinal and lateral slip is employed due to the capability of this model to simulate the limit handling situations where strong nonlinearity is present.

BLDC Motor Model

BLDC motor [16] is one kind of permanent magnet synchronous motor, with permanent magnets on the rotor and trapezoidal shape back EMF (electromotive forces). The BLDC motor employs a DC power supply switched to the stator phase windings of the motor by power devices, the switching sequence being determined from the rotor position. The phase current of BLDC motor, typically in a rectangular shape, is synchronized with the back EMF to produce constant torque at a constant speed. BLDC motors have higher efficiency compared with brushed DC motor due to the elimination of magnetizing current and copper loss in the rotor. It is also easier to achieve high-performance torque control with them. Owing to these advantages, BLDC motors have been widely used in a variety of applications in industrial automation and consumer electric appliances. Recent advancements in permanent magnetic materials have made the PM (permanent magnet) motor a great candidate for traction motors in electrical vehicle applications. The BLDC motor used here has 4 magnetic pole pairs on the rotor and a three-phase star connected with windings on stator. The governing Equations of BLDC motor can be represented as:

$$\begin{cases} \frac{d}{dt} i_a = \frac{1}{3L_s}\left(2V_{ab} + V_{bc} - 3R_s i_a - 2E_a + E_b + E_c\right) \\ \frac{d}{dt} i_b = \frac{1}{3L_s}\left(-V_{ab} + V_{bc} - 3R_s i_b + E_a - 2E_b + E_c\right) \\ \frac{d}{dt} i_c = -\frac{d}{dt}\left(i_a + i_b\right) \end{cases} \quad (2)$$

Where V_{ab} and V_{bc} are '*ab*' and '*bc*' phase to phase voltages, R_s and L_s are phase resistance and inductance; i_a , i_b , and i_c are phase currents and E_a, E_b, and E_c are back EMFs. The induced EMF are all assumed to be trapezoidal, given by:

$$\begin{cases} E_a = p\lambda_m \phi_a\left(\theta_e\right)\omega_m \\ E_b = p\lambda_m \phi_b\left(\theta_e\right)\omega_m \\ E_c = p\lambda_m \phi_c\left(\theta_e\right)\omega_m \end{cases} \quad (3)$$

Where λ_m is amplitude of the flux induced by the permanent magnets of the rotor in the stator phases; *p* is number of pole pairs; $\phi_a\left(\theta_e\right), \phi_b\left(\theta_e\right)$, and $\phi_c\left(\theta_e\right)$ are functions having the same shapes as back EMF with a maximum magnitude of ± 1. Electrical rotor position θ_e and rotor speed ω_e can be defined as:

$$\begin{cases} \theta_e = p\theta_m \\ \omega_e = p\omega_m \end{cases} \quad (4)$$

Where θ_m and ω_m are mechanical rotor angular position and angular speed, respectively. The generated electromagnetic torque is given by:

$$T_e = \frac{E_a i_a + E_b i_b + E_c i_c}{\omega_m} = p\lambda_m\left(\phi_a i_a + \phi_b i_b + \phi_c i_c\right) \quad (5)$$

The mechanical angular acceleration of rotor is given by:

$$\dot{\omega}_m = \frac{1}{J_m}\left(T_e - B_m\omega_m - T_m\right) \quad (6)$$

Where J_m is the mass moment inertia of the rotor about the axis of rotation, B_m is viscous friction coefficient and T_m is shaft mechanical torque applied on rotor. The parameters characterizing BLDC motor are shown in "Table 1".

Table1 Parameters characterizing BLDC motor

V_{dc}	L_s	λ_m	R_s	p
240	8.5e-3	0.192	0.05	4

3 CONTROLLER DESIGN

Upper Layer Controller

The controller gives the desired torque that BLDC motor should produce. To improve the system's robustness, given the presence of modeling uncertainties, a sliding mode controller (SMC) has been considered. The BLDC motor is connected to a reduction gear system, so the angular speed and torque of the motor and wheel are related by:

$$\omega = \frac{\omega_m}{n} \quad T_w = nT_m \quad (7)$$

Where n is the reduction ratio. Substituting "Eqs. (6) and (7)" into "Eq. (1)" yields:

$$\dot{\omega} = \frac{1}{J_{eq}}\left(nT_e - B_{eq}\omega - T_L\right) \tag{8}$$

Where:

$$J_{eq} = J_w + n^2 J_m \quad B_{eq} = n^2 B_m \quad T_L = F_x R + F_z d$$

The wheel slip in the vehicle accelerating mode is given as:

$$\lambda = 1 - \frac{U_w}{R\omega} \tag{9}$$

Differentiating "Eq. (9)" with respect to time gives the derivative form:

$$\dot{\lambda} = \frac{U_w}{R\omega^2}\dot{\omega} - \frac{\dot{U_w}}{R\omega} \tag{10}$$

Substituting "Eq. (8)" into "Eq. (10)" and using the longitudinal acceleration of the vehicle instead of a wheel, the nonlinear first-order differential Equation of wheel slip is obtained as:

$$\dot{\lambda} = \frac{(1-\lambda)}{J_{eq}\omega}\left(nT_e - B_{eq}\omega - T_L - \frac{J_{eq}}{(1-\lambda)}\frac{a_x}{R}\right) \tag{11}$$

The control objective is to drive the state λ to the reference value λ_d. In accordance with the typical methodology of the design of the SMC system, the following definition for the sliding surface s has been given:

$$s = \lambda - \lambda_d \tag{12}$$

The sliding law is defined as [17]:

$$\dot{s} = -K\ \mathrm{sgn}(s) \tag{13}$$

Where, K is the controller gain and the discontinuous switching function $\mathrm{sgn}(s)$ can result in chattering during the sliding motion. In general, chattering must be eliminated for the controller to perform properly. A solution to this problem is to replace the discontinuous switching with smooth, continuous switching, such as the saturation function defined as:

$$\mathrm{sat}\left(\frac{s}{\phi}\right) = \begin{cases} \mathrm{sgn}(s) & \left|\frac{s}{\phi}\right| > 1 \\ \frac{s}{\phi} & \left|\frac{s}{\phi}\right| < 1 \end{cases} \tag{14}$$

Where ϕ, is a design parameter denoting the boundary layer thickness. The sliding mode controller law could be stated by using "Eqs. (11), (12), (13), and (14)" as:

$$T_e = \frac{1}{n}\{B_{eq}\omega + \frac{J_{eq}}{(1-\lambda)}\frac{a_x}{R} + T_L + \frac{J_{eq}\omega}{(1-\lambda)}\dot{\lambda}_d - \frac{J_{eq}\omega}{(1-\lambda)}K\ \mathrm{sat}\left(\frac{\lambda-\lambda_d}{\phi}\right)\} \tag{15}$$

The torque given by "Eq. (15)" is the desired value for the lower controller, which will be described in the next section.

Lower Layer controller

Figure 3 illustrates the block diagram of a torque control scheme for a BLDC motor drive.

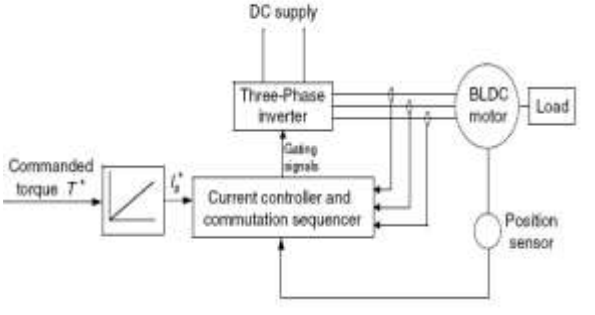

Fig. 3 Torque control of a BLDC motor drive [1].

The desired current I_s^* is derived from the commanded torque T^* through the upper layer controller. The current controller and commutation sequencer receive the desired current I_s^* position information from the position sensors, and the current feedback through current transducers, and then produce gating signals. These gating signals are sent to the three-phase inverter (power converter) to produce the phase current desired by the BLDC machine. The three-phase inverter consists of six transistors connected in a bridge form. The structure of the inverter is shown in "Fig. 4". The same information is presented in "Table 2".

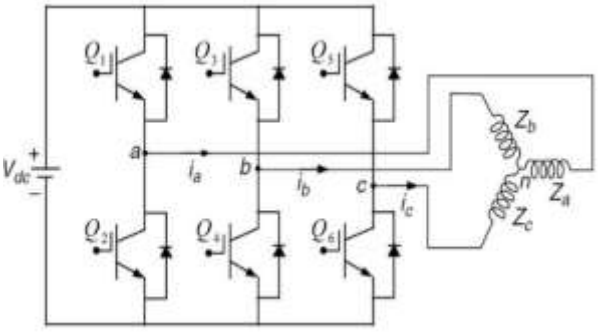

Fig. 4 Three-phase BLDC Power Stage.

Table2 Six step commutation sequence

Hall effect sensor value $(H_a H_b H_c)$	Phase	Switches
101	*a-b*	Q_1; Q_4
100	*a-c*	Q_1; Q_6
110	*b-c*	Q_3; Q_6
010	*b-a*	Q_3; Q_2
011	*c-a*	Q_5; Q_2
001	*c-b*	Q_5; Q_4

The BLDC motor is equipped with three Hall effect sensors. This signal is very useful to control directly the power switches. The Hall-effect sensors produce three 180-degree (electrical) overlapping signals as shown in "Fig. 4". The Hall effect signal provides a logical indication of the back EMF positioning; thus, it provides six mandatory commutation points. The Hall effect sensor outputs are directly connected to the current controller. These signals must be decoded before being applied to the switches to generate the necessary switching sequence as per commutation.

Figure 5 and "Table 2" show that during any 120-degree interval of electrical rotation, two phases are conducting, so from "Eq. (5)", the desired current of torque control is obtained as [16]:

$$I_s^* = \frac{T^*}{2p\lambda_m} \tag{16}$$

By multiplying the desired current I_s^* with the decoded Hall effect sensor signals, the desired current in each of the three phases can be obtained. The PWM width is determined by comparing the measured actual current with the desired reference current in any phase. The logic used by the current controller is to drive the actual current to the desired value. For example, the controller that controls phase '*a*', it checks to see whether the actual current in phase '*a*' is greater than the required current; if it is, then it will activate transistor Q_2. Otherwise, it will activate transistor Q_1.

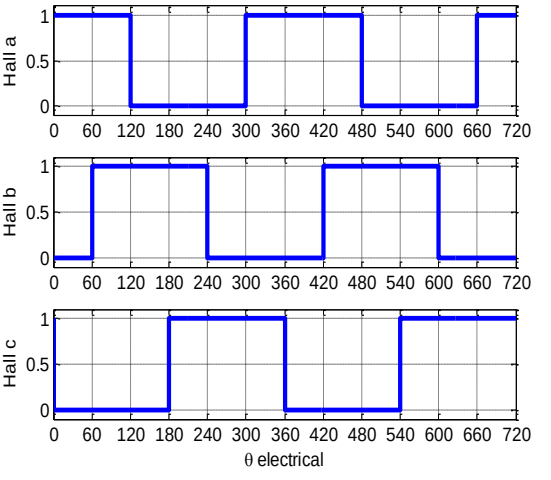

Fig. 5 Hall effect sensor output in 720-degree electrical rotation.

4 SIMULATIONS

In this section, the proposed control system is simulated using MATLAB/Simulink software. The simulations performed are straight-line maneuvers where the reference input wheel slip on each wheel is constant. The simulations include acceleration maneuvers on different road conditions. Table 3 shows the simulation parameters for the sliding mode controller.

Table 3 The simulation parameters

ϕ	K
0.1	20

In the first simulation, the vehicle is accelerating on a dry road with reference wheel slip, $\lambda_d = 0.1$, which is the desired value for maximum acceleration. Simulation results for the first maneuver are shown in "Figs. 6 to 9". Figure 6 shows the actual and desired wheel slip, while "Fig. 7" illustrates the wheel slip tracking error. The desired torque calculated by the sliding mode controller and the torque generated by BLDC motor via the current controller are shown in "Fig. 8". It is evident from "Fig. 6" that the actual slip follows the desired value precisely. However, as depicted in "Fig. 7", the tracking error is quite "noisy" which is expected when using PWM inverters. The noise introduced by the PWM inverter is also noticeable in the electromagnetic torque waveform. Additionally, "Fig. 9" demonstrates the stepped square shape of the motor currents, a result of the DC bus applying a constant voltage to the motor inductances during 120 electrical degrees.

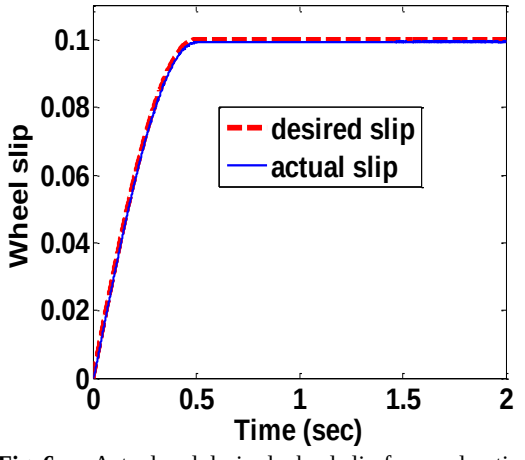

Fig. 6 Actual and desired wheel slip for accelerating on dry road.

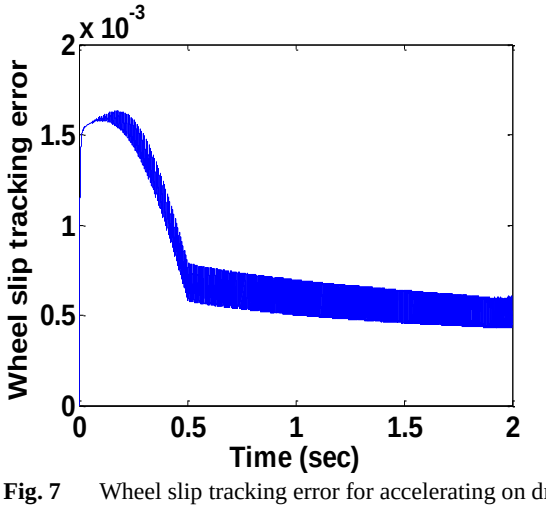

Fig. 7 Wheel slip tracking error for accelerating on dry road.

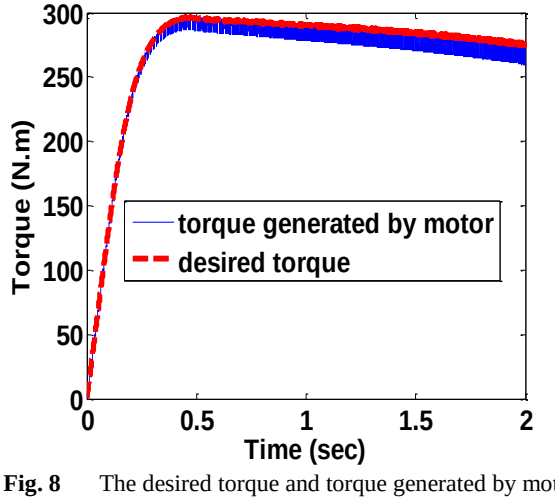

Fig. 8 The desired torque and torque generated by motor for accelerating on dry road.

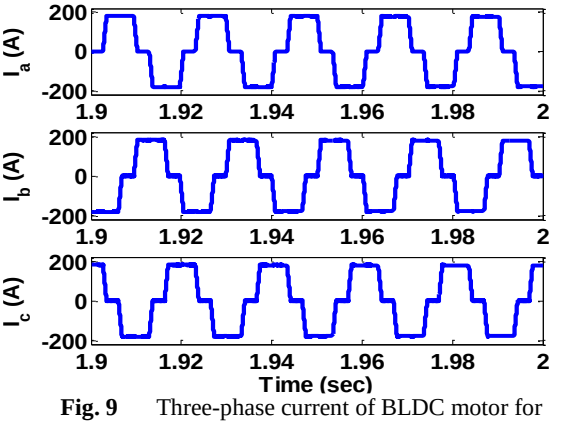

Fig. 9 Three-phase current of BLDC motor for accelerating on dry road.

In the second simulation, the vehicle is accelerating on a slippery road (μ = 0.4), with reference wheel slip, $\lambda_d = 0.1$, which is the desired value for maximum acceleration on a slippery road without wheel spinning. Simulation results for the second maneuver are shown in "Figs. 10 to 13".

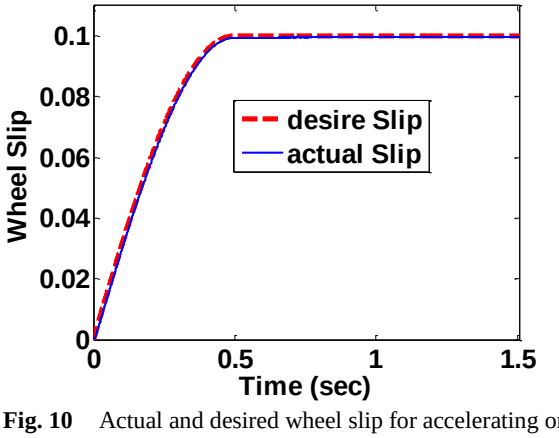

Fig. 10 Actual and desired wheel slip for accelerating on slippery road.

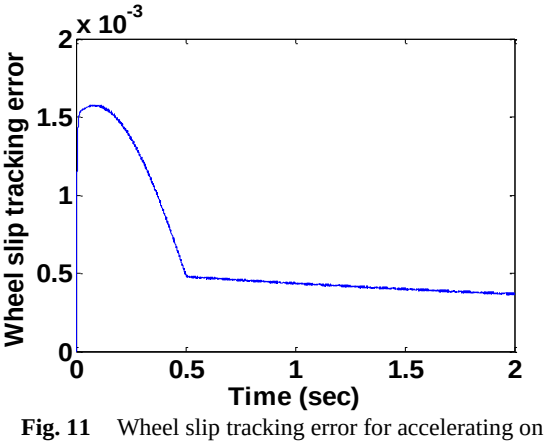

Fig. 11 Wheel slip tracking error for accelerating on slippery road.

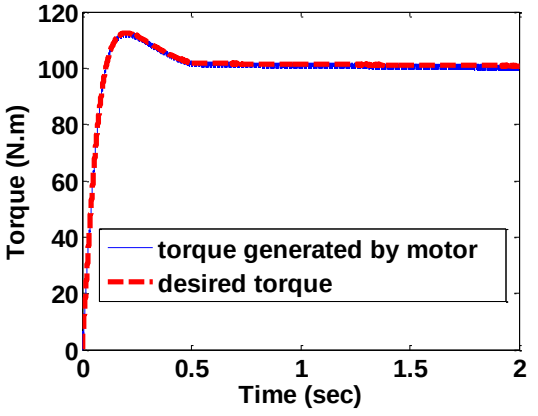

Fig. 12 The desired torque and torque generated by the motor for accelerating on a slippery road.

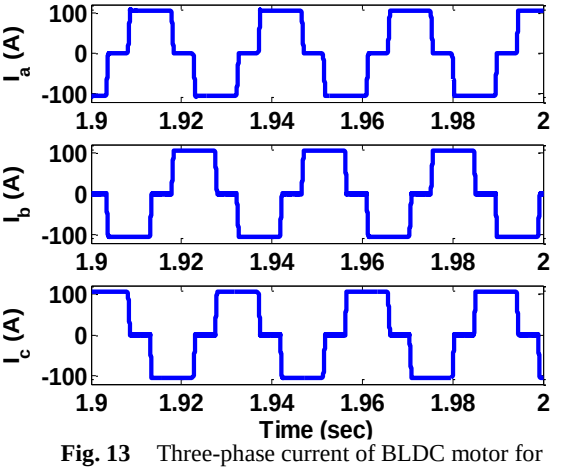

Fig. 13 Three-phase current of BLDC motor for accelerating on slippery road.

As depicted in "Figs. 10 and 11", the slip controller effectively tracks slip in slippery conditions. Additionally, "Figs. 12 and 13" demonstrate that the motor torque during the first maneuver on a dry road is higher compared to the torque on a slippery road. This is due to the reduced load torque applied to the wheel on slippery surfaces. Consequently, the phase current is also lower in comparison to the previous scenario.

5 CONCLUSIONS

In this paper, a sliding mode control strategy for controlling wheel slip with an in-wheel electric motor has been developed. This controller may be part of a vehicle dynamics stability system for in-wheel electric vehicles. The control objective is to track a reference wheel slip. To achieve this, a two-layer controller is proposed in such a way that the upper-layer controller tracks the slip reference using sliding mode and provides the desired torque for the lower-layer controller. The controller requires information on the longitudinal tire forces, which can be obtained through actual sensor signals or observers. The lower controller is the torque controller for the BLDC motor, which operates by controlling the motor's current to achieve the desired torque. The precise results of computer simulations demonstrate the good performance of the proposed control system under both normal and severe road conditions.

REFERENCES

[1] Ehsani, M., Gao, Y., and Emadi, A., Modern Electric, Hybrid Electric, and Fuel Cell Vehicles: Fundamentals, Theory, and Design, 2nd ed., CRC Press, Taylor & Francis Group, Boca Raton, Florida, USA, 2010.

[2] Chen, Y., Hedrick, J. K., and Guo, K., A Novel Direct Yaw Moment Controller for In-Wheel Motor Electric Vehicles, Vehicle System Dynamics, Vol. 51, No. 6, 2013, pp. 925-942, doi: 10.1080/00423114.2013.773453.

[3] Hu, J. S., Wang, Y., Fujimoto, H., and Hori, Y., Robust Yaw Stability Control for In-Wheel Motor Electric Vehicles, IEEE/ASME Transactions On Mechatronics, Vol. 22, No. 3, 2017, pp. 1360-1370, doi: 10.1109/TMECH.2017.2677998.

[4] Majidi, M., Asiabar, A. N., Stability Enhancement of In-Wheel Motor Drive Electric Vehicle Using Adaptive Sliding Mode Control, ADMT Journal, Vol. 15, No. 2, 2022, pp. 23-33, doi: 10.30486/admt.2022.1938721.1311.

[5] Shino, M., Nagai, M., Yaw-Moment Control of Electric Vehicle for Improving Handling and Stability, JSAE Review, Vol. 22, No. 4, 2001, pp. 473-480, doi: 10.1016/S0389-4304(01)00130-8.

[6] Shino, M., Nagai, M., Independent Wheel Torque Control of Small-Scale Electric Vehicle for Handling and Stability Improvement, JSAE Review, Vol. 24, No. 4, 2003, pp. 449-456, doi: 10.1016/S0389-4304(03)00080-8.

[7] Wang, Z., Wang, Y., Zhang, L., and Liu, M., Vehicle Stability Enhancement Through Hierarchical Control for A Four-Wheel-Independently-Actuated Electric Vehicle, Energies, Vol. 10, No. 7, 2017, pp. 947, doi: 10.3390/en10070947.

[8] Pande, S. D., and *et al.*, A Fuzzy-Based Slip Resistive Controller for Front Wheel Drive Autonomous Electric Vehicle, Electric Power Components and Systems, Vol. 52, No. 10, 2024, pp. 1821-1831.

[9] He, Z., Shi, Q., Wei, Y., Gao, B., Zhu, B., and He, L., A Model Predictive Control Approach With Slip Ratio Estimation for Electric Motor Antilock Braking of Battery Electric Vehicle, IEEE Transactions on Industrial Electronics, Vol. 69, No. 9, 2021, pp. 9225-9234.

[10] Mirzaeinejad, H., Mirzaei, M., A Novel Method for Non-Linear Control of Wheel Slip in Anti-Lock Braking Systems, Control Engineering Practice, Vol. 18, No. 8, 2010, pp. 918-926, doi: 10.1016/j.conengprac.2010.03.015.

[11] De Castro, R., Araújo, R. E., Tanelli, M., Savaresi, S. M., and Freitas, D., Torque Blending and Wheel Slip Control in Evs with In-Wheel Motors, Vehicle System Dynamics, Vol. 50, No. 1, 2012, pp. 71-94, doi: 10.1080/00423114.2012.666357.

[12] Yuan, L., Zhao, H., Chen, H., and Ren, B., Nonlinear MPC-Based Slip Control for Electric Vehicles with Vehicle Safety Constraints, Mechatronics, Vol. 38, 2016, pp. 1-15, doi: 10.1016/j.mechatronics.2016.05.006.

[13] Mashadi, B., Majidi, M., Integrated AFS/DYC Sliding Mode Controller for A Hybrid Electric Vehicle, International Journal of Vehicle Design, Vol. 56, No. 1-4, 2011, pp. 246-269, doi: 10.1504/IJVD.2011.043268.

[14] He, J., Crolla, D. A., Levesley, M., and Manning, W., Coordination of Active Steering, Driveline, and Braking for Integrated Vehicle Dynamics Control, Proceedings of the Institution of Mechanical Engineers, Part D: Journal of Automobile Engineering, Vol. 220, No. 10, 2006, pp. 1401-1420, doi: 10.1243/09544070JAUTO265.

[15] Pacejka, H., Tire and Vehicle Dynamics, Elsevier, 2005.

[16] Murugan, R., Nandakumar, S., and Mohiyadeen, M., DSP-Based Electric Power Assisted Steering Using BLDC Motor, Sadhana, Vol. 33, 2008, pp. 581-590, doi: 10.1007/s12046-008-0044-z.

[17] Slotine, J. J. E., Li, W., Applied Nonlinear Control, Prentice Hall, Englewood Cliffs, NJ, USA, 1991.